

Dynamics of turbulent helium II, limits of the Vinen model

T. LIPNIACKI (WARSZAWA)

THE DYNAMICS of superfluid helium is considered within the framework of the Vinen model. According to Vinen equation, counterflow (the relative velocity of the two helium components) gives rise to quantum turbulence. The mutual friction force, exerted on the vortex tangle by the normal component, couples it with the superfluid component. The system of 3 ordinary equations is numerically solved to calculate the characteristic entrainment time in which the counterflow ceases. For the typical velocities of order 1 cm/s, the entrainment time is found to be much smaller than the vorticity diffusion time for the length scale of 1 cm. It suggests that in the typical spin-up experiments the quantum turbulence plays a key role coupling the two components. Unfortunately the Vinen model applied to spin-up turned out to be inconsistent; the vortex line density calculated from the superfluid component vorticity was found to be much larger than that predicted by the Vinen equation.

1. Introduction

THE LANDAU'S two-fluid theory [1] has proved to be indispensable for understanding of the peculiar flow properties of ^4He below the λ -point. In the two-fluid theory He II (superfluid ^4He) is a sum of the Bose condensate (superfluid component) and the gas of thermal excitation (normal component). Densities of superfluid and normal components ϱ_s , ϱ_n respectively, are temperature-dependent and satisfy

$$(1.1) \quad \varrho = \varrho_n + \varrho_s,$$

where ϱ denotes the total mass density of the liquid.

The theory was later improved by ONSAGER [2] and FEYNMAN [3] who found that Landau's assumption of rotationless flow of the superfluid component was violated on one-dimensional singularities called now quantum vortices. The circulation of the superfluid velocity about these lines remains constant, $\kappa = h/m_{\text{He}} = 9.97 \cdot 10^{-4} \text{ cm}^2/\text{s}$, where h is Planck's constant, and m_{He} is the mass of helium atom. The interaction between the vortices and the elementary excitation couples the normal and superfluid components. Within the limits of that de facto three-fluid theory, two main models were proposed:

1) the VINEN model [4] which describes helium in the state of a superfluid turbulence, when the quantum vortices form an irregular tangle, and

2) the Hall–Vinen–Bekarevich–Khalatnikov [5] (HVBK) model concerning the case when moving vortices form a regular pattern of parallel orientation (superfluid laminar flow).

When the magnitude of relative velocity $V_{ns} = |V_n - V_s|$ gets sufficiently large, superfluid laminar flow develops into superfluid turbulent flow. It significantly restricts the usage of the HVBK model.

The easiest way of generating a sizable V_{ns} is to seal one end of the channel and place a heater there. The normal fluid produced by the heater flows out of the channel with an average velocity V_n proportional to the heat input to the channel. The normal fluid moving away from the heater is replaced by a superfluid flowing in the opposite direction, the superfluid velocity V_s being determined by the condition of zero mass transport $\varrho_s V_s + \varrho_n V_n = 0$.

Because there is a variety of observations on superfluid turbulence caused by heat flows in a counterflow channel, the Vinen model has been usually connected with the problems of the heat transport. In fact not only the heat transfer may cause the counterflow.

For example the viscous forces in a rotating cylinder or a moving channel may give rise to the difference in the components velocities. The calculations show that even the relative velocity of order 1 cm/s may cause the quantum turbulence strong enough to influence the dynamics of the two components.

To study this problem in more detail, we recall basic facts of the Vinen model according to the approach developed by SCHWARZ [6, 7]. We use the modified vortex-line-length density L_m

$$(1.2) \quad L_m = (I_{||} - c_L I_l) L,$$

where L is the total line-length density (i.e. the length of vortices per unit of volume). $(I_{||} - c_L I_l)$ is a coefficient describing vortex tangle anisotropy and is equal to $2/3$ for isotropic tangle. The modified density was introduced by Schwarz as a quantity which can be directly measured in thermal-counterflow experiments.

The time evolution of the modified vortex-line-length density is governed by Vinen-type equation

$$(1.3) \quad \frac{dL_m}{dt} = \alpha I_{lm} \left(V_{ns} L_m^{3/2} - \frac{\beta}{c_{Lm}} L_m^2 \right),$$

where I_{lm} , c_{Lm} are temperature-dependent dimensionless coefficients, α is the friction coefficient, and β is defined by

$$(1.4) \quad \beta = \frac{\kappa}{4\pi} \ln \left(\frac{c}{a_0 \langle s'' \rangle} \right) \approx \kappa,$$

where κ is the quantum of circulation, c is a constant of order one, $\langle s'' \rangle$ is the average curvature of the vortices in the tangle and $a_0 \simeq 1.3 \cdot 10^{-8}$ cm is the effective core radius of a quantized vortex. Although β has the logarithmic dependence on the tangle density since $\langle s'' \rangle$ increases as the tangle density increases, it can usually be treated as a constant. For the typical tangle densities we can replace everywhere β by κ . The values of the dimensionless parameters used

in that paper, based on numerical simulations by SCHWARZ [6] (from GEURST and BEELEN [8]), are presented in the Table 1. The thermal excitation (phonons and rotons) exerts the force on the quantized vortices of a vortex tangle, what gives rise to the friction force between the two components. The density of that force is F_{ns}

$$(1.5) \quad F_{ns} = \varrho_s \kappa \alpha L_m V_{ns}.$$

Table 1. Values of dimensionless parameters [8] and kinematic viscosity ν_n [cm²/s].

Temp.	1.07	1.26	1.62	2.01	2.15
ϱ_n/ϱ	0.013	0.039	0.174	0.576	0.886
α	0.010	0.030	0.100	0.300	1.00
$I_{ } - c_L I_l$	0.70	0.72	0.71	0.77	0.85
I_{lm}	0.51	0.52	0.54	0.52	0.39
c_{Lm}	0.031	0.062	0.11	0.19	0.26
c_I	0.061	0.12	0.20	0.36	0.67
ν_n	$1.5 \cdot 10^{-2}$	$3.0 \cdot 10^{-3}$	$5.1 \cdot 10^{-4}$	$1.8 \cdot 10^{-4}$	$1.7 \cdot 10^{-4}$

In incompressible approximation $\text{div } V_n = \text{div } V_s = 0$, the dynamical equations are [9]

$$(1.6) \quad \begin{aligned} \varrho_n \left(\frac{\partial V_n}{\partial t} + V_n \nabla V_n \right) + \nabla p_n &= \nu_n \Delta^2 V_n - F_{ns}, \\ \varrho_s \left(\frac{\partial V_s}{\partial t} + V_s \nabla V_s \right) + \nabla \mu &= F_{ns}, \end{aligned}$$

where

$$(1.7) \quad p_n = \frac{p}{\varrho_n} - \frac{\varrho_n \mu}{\varrho_s}$$

and p , ν_n , μ are pressure, kinematic viscosity of the normal component and chemical potential, correspondingly.

We illustrate the applications of Vinen model solving 3 simple problems.

2. Thermal-counterflow

The switched on heater power gives rise to a counterflow of the prescribed velocity V_{ns} (the inertia forces are neglected). According to Eq. (1.3), the counterflow makes the vortex line-length density to start growing from the initial value L_0 to the asymptotic one L_f

$$(2.1) \quad L_f = \left(\frac{c_{Lm}}{\kappa} \right)^2 V_{ns}^2.$$

Then at the given time, the heater power is switched off ($V_{ns} = 0$) and the vortex line-length density sharply decreases. The solution $L_m(t)$ to equation (1.3) is shown in the Fig. 1. The characteristic tangle production time T_{prod} in which the vortex line-density reaches half of its asymptotic value is

$$(2.2) \quad T_{\text{prod}} = \int_{L_0}^{L_f/2} \frac{dl}{\alpha I_{lm} \left(V_{ns} L_m^{3/2} - \frac{\kappa}{c_{Lm}} L_m^2 \right)} \simeq \frac{2}{\alpha I_{lm} V_{ns} L_0^{1/2}}.$$

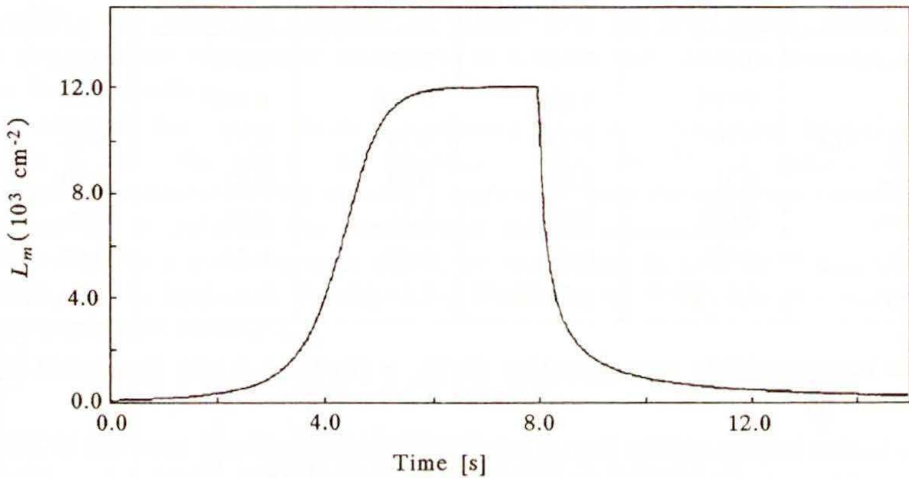


FIG. 1. Rise and decrease of vortex tangle density. At the time $t = 0$ heater power is switched on causing the thermal-counterflow of value 1 cm/s, then at the time $t = 8$ s heater power is switched off and the vortex line-length density sharply decreases. Temp. = 1.62° K.

The tangle production time is inversely proportional to the root of the initial vortex line-density, which can be small if the helium was left in peace for a long time, but even after very long time some remnant vortices are present. The minimum line-density observed value was 10 cm^{-2} , while the typical value for the superfluid turbulence is $10^3 \sim 10^7 \text{ [cm}^{-2}]$.

3. Entrainment Problem (1)

Here we restrict ourselves to the case in which the component velocities and the line-length density are only time-dependent. Let us assume that in the initial state the normal component is moving with the uniform velocity V_0 , while the superfluid component remains at rest. The initial line-length density L_0 is assumed to be small when compared to the asymptotic value L_f for the steady

counterflow $V_{ns} = V_0$. The system is described by the set of 3 ordinary equations

$$(3.1) \quad \begin{aligned} \frac{dV_n}{dt} &= -\frac{\varrho_s \kappa \alpha L_m (V_n - V_s)}{\varrho_n}, \\ \frac{dV_s}{dt} &= \kappa \alpha L_m (V_n - V_s), \\ \frac{dL_m}{dt} &= \alpha I_{lm} \left(|V_n - V_s| L_m^{3/2} - \frac{\kappa}{c_{Lm}} L_m^2 \right). \end{aligned}$$

To rewrite the equations in the dimensionless form we introduce new variables

$$(3.2) \quad v_n = \frac{V_n}{V_0}, \quad v_s = \frac{V_s}{V_0}, \quad l = \frac{L_m}{L_f},$$

where L_f is the asymptotic value for the steady counterflow $V_{ns} = V_0$ given in Eq. (2.1).

Then we have

$$(3.3) \quad \begin{aligned} \frac{dv_n}{dt} &= -\frac{1}{T_{ns}} \frac{l(v_n - v_s) \varrho_s}{\varrho_n}, \\ \frac{dv_s}{dt} &= \frac{1}{T_{ns}} L_m (v_n - v_s), \\ \frac{dl}{dt} &= \frac{1}{T_l} l^{3/2} \left(|v_n - v_s| - l^{1/2} \right), \end{aligned}$$

where T_{ns} , T_l are the characteristic times defined as follows:

$$(3.4) \quad \begin{aligned} T_{ns} &= \kappa \alpha^{-1} c_{Lm}^{-2} V_0^{-2}, \\ T_l &= \kappa \alpha^{-1} c_{Lm}^{-1} V_0^{-2} I_{lm}. \end{aligned}$$

T_l is the characteristic time scale of line density changes (when the density is of order L_f) and should not be confused with T_{prod} which is the time scale for the line-length density growth from a small initial value.

Introducing the new time $\tau = t/T_l$ we obtain

$$(3.5) \quad \begin{aligned} \frac{dv_n}{d\tau} &= -c_I \frac{l(v_n - v_s) \varrho_s}{\varrho_n}, \\ \frac{dv_s}{d\tau} &= c_I l (v_n - v_s), \\ \frac{dl}{d\tau} &= l^{3/2} \left(|v_n - v_s| - l^{1/2} \right), \end{aligned}$$

where

$$(3.6) \quad c_I = \frac{T_l}{T_{ns}} = \frac{c_{Lm}}{I_{lm}}$$

is the dimensionless temperature-dependent parameter.

The problem can be further reduced to the set of two equations

$$(3.7) \quad \begin{aligned} \frac{dv_{ns}}{d\tau} &= Clv_{ns}, \\ \frac{dl}{d\tau} &= l^{3/2} (|v_{ns}| - l^{1/2}), \end{aligned}$$

with $v_{ns} = v_n - v_s$ and $C = c_I(\varrho_n + \varrho_s)/\varrho_n$. Multiplying Eq. (3.7)₁ by v_{ns} one can see that v_{ns}^2 is not growing, so v_{ns} may not change the sign. It is enough to consider the case $v_{ns} \geq 0$ since the case $v_{ns} \leq 0$ is identical. The points ($l = 0$, v_{ns} - arbitrary) are invariant points to the set of Eq. (3.7). Although the case $l = 0$ is unphysical since some remnant vortices are always present, it may be still interesting to see if the manifold $l = 0$ is stable. Since $dl/d\tau > 0$ for $0 < l < v_{ns}^2$ all the points ($l = 0$, $v_{ns} > 0$) are unstable. The point ($l = 0$, $v_{ns} = 0$) is stable, moreover all trajectories starting from points ($l \neq 0$) tend to it. To prove the last fact it is enough to solve the following equations resulting from Eq. (3.7)

$$(3.8) \quad \frac{dl}{dv_{ns}} = K \left(\frac{l}{v_{ns}} - l^{1/2} \right),$$

with $K = 1/C$. Its solution is

$$(3.9) \quad l = (v_{ns})^K \left(\frac{K(v_{ns})^{(1-K/2)}}{K-2} + C_0 \right)^2.$$

Now from Eq. (3.7)₁ we see that for positive l , v_{ns} tends to zero, and from Eq. (3.9) that l tends to zero with v_{ns} tending to zero. The last solution can be put into Eq. (3.7)₁ and then the equation is integrated.

The solutions to Eqs. (3.5) for 3 various temperatures and $V_0 = 1$ cm/s, $L_0 = 100$ cm⁻² are presented in Figs. 2–4. One can see that due to the initial relative velocity, the vortex line-length density grows up. Then the friction force (F_{ns}) makes the relative velocity decrease and may not sustain the vortex tangle, so the vortex line density decreases. The characteristic time T_{ent} in which the relative velocity V_{ns} is reduced e times from its initial value to V_0/e , decreases with increasing temperature. It is also worth to notice that since

$$(3.10) \quad T_{ns} \sim V_0^{-2}, \quad T_l \sim V_0^{-2},$$

hence

$$(3.11) \quad T_{ent} \sim V_0^{-2}.$$

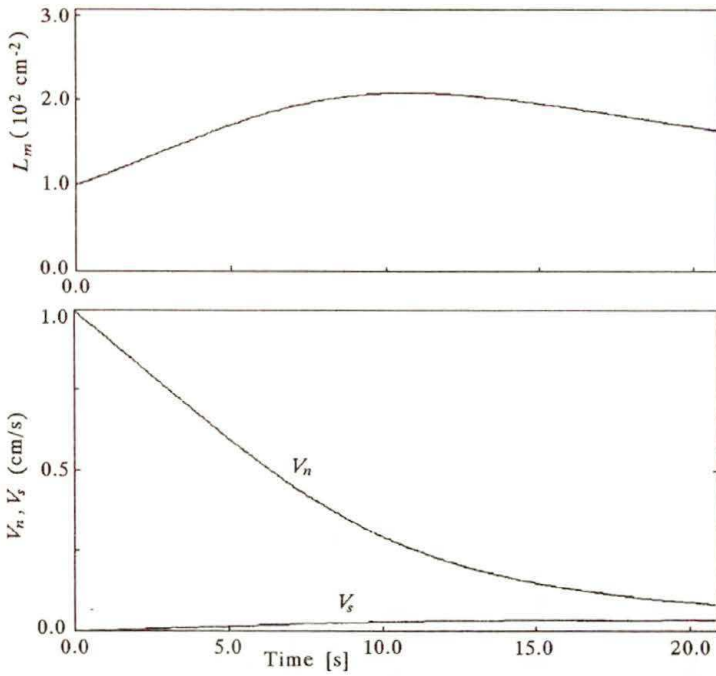


FIG. 2. Numerical solutions for the entrainment problem equations with the initial values $V_0 = 1$ cm/s, $L_0 = 100$ cm $^{-2}$. Temp. = 1.26° K.

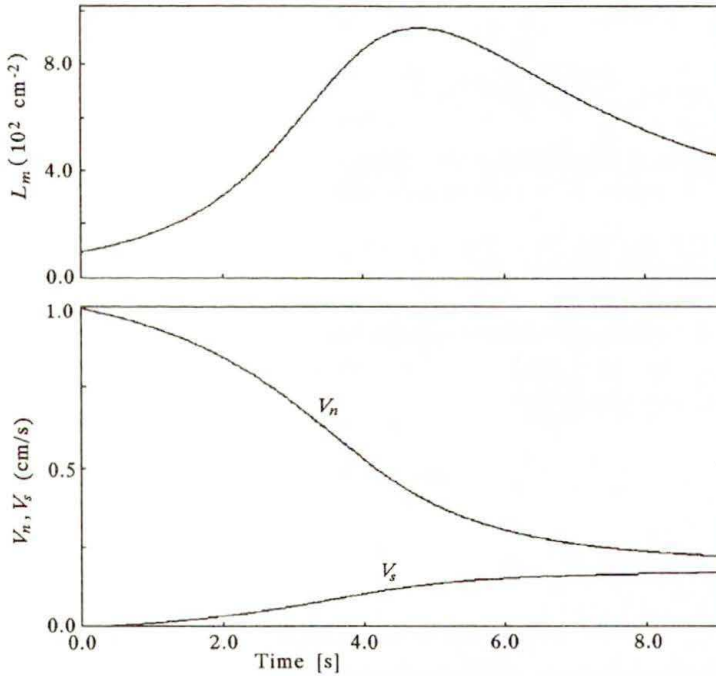


FIG. 3. Numerical solutions for the entrainment problem equations with the initial values $V_0 = 1$ cm/s, $L_0 = 100$ cm $^{-2}$. Temp. = 1.62° K.

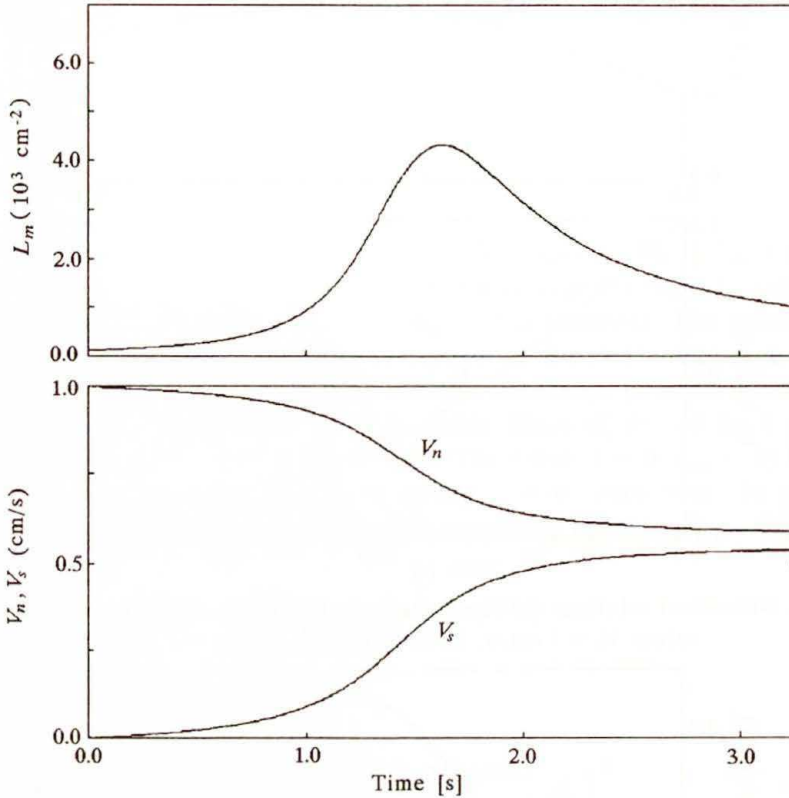


FIG. 4. Numerical solutions for the entrainment problem equations with the initial values $V_0 = 1$ cm/s, $L_0 = 100$ cm². Temp. = 2.01° K.

4. Entrainment problem (2)

Another interesting problem arises when the normal component velocity V_s is fixed in time (for example by strong viscous forces). Then the problem reduces to the set of two equations

$$(4.1) \quad \begin{aligned} \frac{dv_s}{d\tau} &= c_I l (1 - v_s), \\ \frac{dl}{d\tau} &= l^{3/2} (|1 - v_s| - l^{1/2}). \end{aligned}$$

Putting $v_{ns} = 1 - v_s$ we get the same equations as (3.7) but with $C = c_I$. Now, for the same temperature the entrainment time (\widetilde{T}_{ent}) is longer. The difference between \widetilde{T}_{ent} and T_{ent} is especially great for low temperatures when $\varrho_s \gg \varrho_n$. The solution to Eqs. (4.1) is given in Fig. 5, while Table 2 presents times \widetilde{T}_{ent} and T_{ent} , and gives values of L_f for the thermal-counterflow problem.

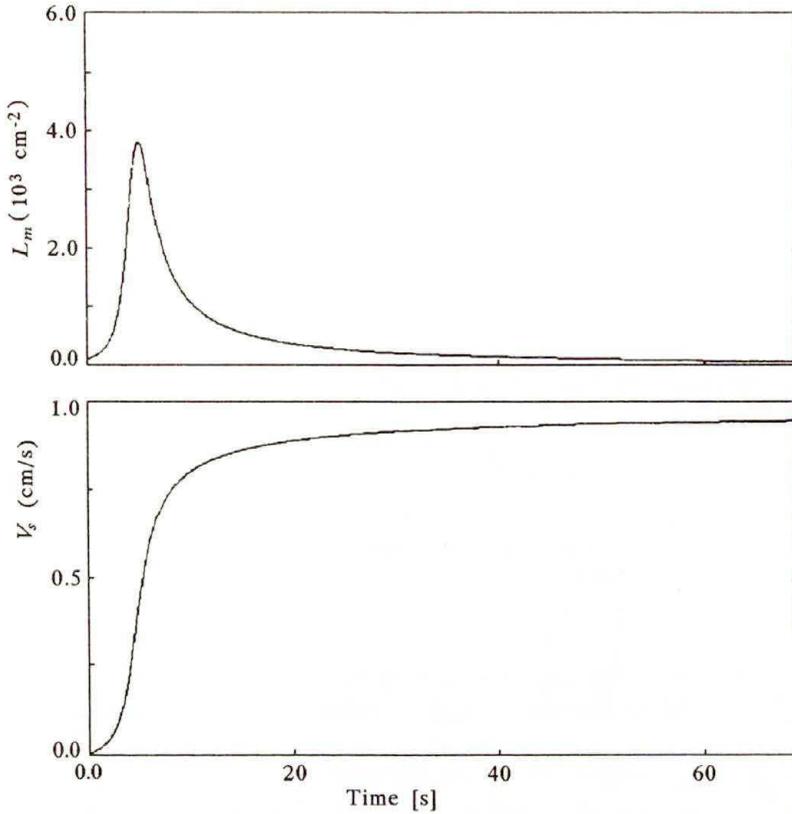


FIG. 5. Numerical solutions for the entrainment problem (2) equations with the initial values $V_0 = 1 \text{ cm/s}$, $L_0 = 100 \text{ cm}^{-2}$. Temp = 1.62° K .

When considering the hydrodynamics of superfluid helium it is important to compare the entrainment times $\widetilde{T}_{\text{ent}}$ and T_{ent} with the characteristic vorticity diffusion time scale

$$(4.2) \quad T_d = \frac{R_0^2}{\nu_n},$$

where $\nu_n = \eta_n/\rho_n$ is the viscosity of the normal component and R_0 is the characteristic length. In Table 2 the entrainment and the diffusion characteristic time scales are compared for various temperatures. When the characteristic relative velocity $V_{ns} = 1 \text{ cm/s}$ and the characteristic size of a helium container $R_0 = 1 \text{ cm}$, the diffusion time is much longer than the entrainment time, especially in a higher temperature. Whereas in very low temperatures, when the normal component is less abundant but more viscous, the two time scales are comparable.

For higher velocities and larger containers the T_d/T_{ent} ratio is even greater. It means that in the larger scale motions, helium II will behave almost like a classical fluid with the overall viscosity $\nu = \eta_n/\rho$. In the finer scale however,

Table 2. Characteristic times [s] ($\widetilde{T}_{\text{ent}}$ and T_{ent} - numerical results for $L_0 = 100 \text{ cm}^{-2}$) and the asymptotic line density [cm^{-2}].

All values are given for $V_0, V_{ns} = 1 \text{ cm/s}$, $\omega = 1/\text{s}$, $R_0 = 1 \text{ cm}$, while appropriate scaling is given in last column.

Temp.	1.07	1.26	1.62	2.01	2.15	scaling
T_{ent}	11.5	8.0	4.3	1.60	0.63	$\sim V^{-2}$
$\widetilde{T}_{\text{ent}}$	310	35	6.3	1.70	0.63	$\sim V^{-2}$
T_l	6.4	1.04	0.17	0.034	0.010	$\sim V^{-2}$
T_{ns}	104	8.8	0.84	0.092	0.015	$\sim V^{-2}$
T_{prod}	39	12.8	3.7	1.28	0.51	$\sim V^{-1}$
T_d	67	330	1960	5550	5880	$\sim R^2$
\widetilde{T}_d	5150	8540	11260	9640	6640	$\sim R^2$
q	0.64	37.8	530	4340	11530	$\sim R^4 \omega^2$
L_f	$9.5 \cdot 10^2$	$3.7 \cdot 10^3$	$1.2 \cdot 10^4$	$3.6 \cdot 10^4$	$6.8 \cdot 10^4$	$\sim V^2$

when the diffusion time is shorter and the smaller velocity may not sustain the quantum turbulence, the two components may move separately.

To see the problem in more detail we analyse the spin-up process focusing on the intermediate scale $V \sim 1 \text{ cm/s}$, $R \sim 1 \text{ cm}$. In the finer scale the Vinen (and any other continuum model) cannot be applied, just because few vortices are expected, and the spacing between the vortices is comparable with the length scale.

5. Analysis of the spin-up in an infinitely long cylinder

We consider here the problem of a spin-up in an infinitely long circular cylinder being impulsively subjected to spinning about its axis of rotation. The case of a finite cylinder is much more complicated because usually the spin-up process is dominated by a secondary flow which transports the vorticity from the boundaries to the center of the cylinder. The secondary flow arises because the fluid at the cylinder ends rotates with the velocity of the wall, and therefore is subject to centrifugal forces which drive it outwards.

In an infinitely long cylinder, the velocity is purely azimuthal and the spin-up of a classical fluid is described by linear equation

$$(5.1) \quad \frac{\partial V}{\partial t} = \nu \frac{\partial^2 V}{\partial r^2} + \frac{\partial}{\partial r} \left(\frac{V}{r} \right),$$

where ν is the kinematic viscosity.

In our case of two fluids, the component velocities $V_n(r, t)$, $V_s(r, t)$ and line length-density $L_m(r, t)$ satisfy the set of 3 differential equations

$$\begin{aligned}
 (5.2) \quad \frac{dV_n}{dt} &= \nu_n \Delta V_n - \frac{\varrho_s \kappa \alpha L_m (V_n - V_s)}{\varrho_n}, \\
 \frac{dV_s}{dt} &= \kappa \alpha L_m (V_n - V_s), \\
 \frac{dL_m}{dt} &= \alpha I_{lm} \left(|V_n - V_s| L_m^{3/2} - \frac{\kappa}{c_{Lm}} L_m^2 \right),
 \end{aligned}$$

where

$$(5.3) \quad \Delta V_n = \frac{\partial^2 V_n}{\partial r^2} + \frac{\partial}{\partial r} \left(\frac{V_n}{r} \right),$$

and $\nu_n = \eta_n / \varrho_n$ is the kinematic viscosity of the normal component. Let us assume that at time $t = 0$ the cylinder of radius R_0 starts to spin about its axis of symmetry with the constant angular velocity ω . The corresponding initial and boundary conditions are

$$\begin{aligned}
 (5.4) \quad V_n(r, 0) &= 0, \quad V_n(R_0, t) = \omega \quad \text{for } r < R_0, \quad t > 0, \\
 V_s(r, 0) &= 0 \quad \text{for } r \leq R_0, \\
 L_m(r, 0) &= L_0 \quad \text{for } r \leq R_0.
 \end{aligned}$$

Again, to rewrite the equations in the dimensionless form we introduce the new variables

$$(5.5) \quad v_n = \frac{V_n}{V_0}, \quad v_s = \frac{V_s}{V_0}, \quad l = \frac{L_m}{L_f},$$

where $V_0 = \omega R_0$ and L_f is the asymptotic value for the steady counterflow $V_{ns} = V_0$

$$(5.6) \quad L_f = \left(\frac{c_{Lm}}{\kappa} \right)^2 (\omega R_0)^2.$$

Then we have

$$\begin{aligned}
 (5.7) \quad \frac{dv_n}{dt} &= \nu_n \Delta v_n - \frac{1}{T_{ns}} \frac{l(v_n - v_s) \varrho_s}{\varrho_n}, \\
 \frac{dv_s}{dt} &= \frac{1}{T_{ns}} l(v_n - v_s), \\
 \frac{dl}{dt} &= \frac{1}{T_l} l^{3/2} (|v_n - v_s| - l^{1/2}),
 \end{aligned}$$

where T_{ns} , T_l are the characteristic times defined as earlier (3.4). Now, let $\xi = r/R_0$.

Introducing the new time variable $\tau = t/T_d$, where

$$(5.8) \quad T_d = \frac{R_0^2}{\nu_n}$$

is the characteristic diffusion time scale, we obtain

$$(5.9) \quad \begin{aligned} \frac{dv_n}{d\tau} &= \Delta_\xi v_n - q \frac{l(v_n - v_s)\rho_s}{\rho_n}, \\ \frac{dv_s}{d\tau} &= ql(v_n - v_s), \\ \frac{dl}{d\tau} &= \frac{q}{c_I} l^{3/2} (|v_n - v_s| - l^{1/2}), \end{aligned}$$

where

$$(5.10) \quad \begin{aligned} \Delta_\xi v_n &= \frac{\partial^2 v_n}{\partial \xi^2} + \frac{\partial}{\partial \xi} \left(\frac{v_n}{\xi} \right), \\ q &= \frac{T_d}{T_{ns}} = \frac{\alpha c_{Lm}^2 R_0^4 \omega^2}{\kappa \nu_n}, \end{aligned}$$

and

$$(5.11) \quad c_I = \frac{T_l}{T_{ns}} = \frac{c_{Lm}}{I_{lm}}$$

is defined as before.

We should notice that while c_I depends on temperature only, parameter q depends on the "experimental conditions" i.e. on the angular velocity and the radius of the cylinder.

When $q \gg 1$ i.e. when there is a strong coupling between the components, the fluid behaves like a classical one satisfying Eq. (5.1) with the overall viscosity $\nu = \eta_n/\rho$. The velocity profile for the classical fluid with the viscosity equal to the overall helium viscosity at $T = 1.62^\circ$ K are reproduced as a reference in Fig. 6.

The numerical solutions to the set of Eqs. (5.9) obtained for $R_0 = 1$ cm, $\omega = 1/s$ for 3 various temperatures are presented in Figs. 7–10.

Figures 7–9 a, b show the velocity profiles of the normal and superfluid components for various temperatures. The line-length density profiles are given in Fig. 10. Figures 7–9 c show the scaled angular momentum m_n , m_s of the two components as a function of time.

$$(5.12) \quad m_s = \frac{M_s}{M_{sf}}, \quad m_n = \frac{M_n}{M_{nf}},$$

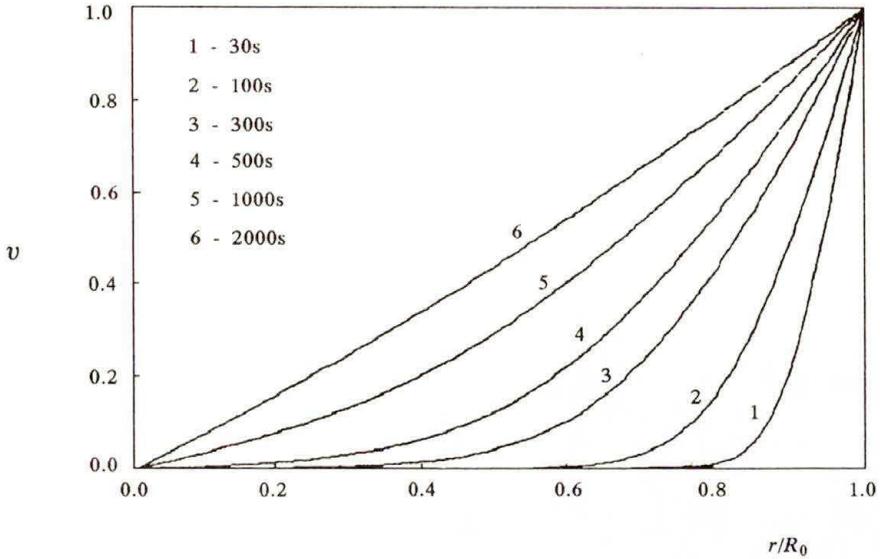


FIG. 6. Evolution of velocity profiles. Classical fluid with viscosity equal to overall viscosity of helium II at 1.62° K.

where the index f means the asymptotic value. Figures 7–9d compare the time evolutions of the total angular momentum for the superfluid and the classical fluid having the same overall viscosity. One can see that for higher temperatures, the total angular momentum of the fluid grows almost as fast as in the classical case.

Table 3. Values of spin-up time T_{spin} for helium II and for classical fluid $\widetilde{T}_{\text{spin}}$ with the same overall viscosity. T_n and T_s are spin-up times for normal and superfluid components, respectively.

Temp.	1.26	1.62	2.01
T_{spin}	450 s	590 s	510 s
$\widetilde{T}_{\text{spin}}$	820 s	830 s	480 s
T_s	840 s	910 s	720 s
T_n	340 s	510 s	880 s

Let us define the spin-up time as a time in which the angular momentum of the fluid reaches 2/3 of its final value. Table 3 compares the spin-up time of the two component fluid with the spin-up time of the classical fluid with the same overall viscosity. The spin-up times of normal and superfluid components are also given for better reference.

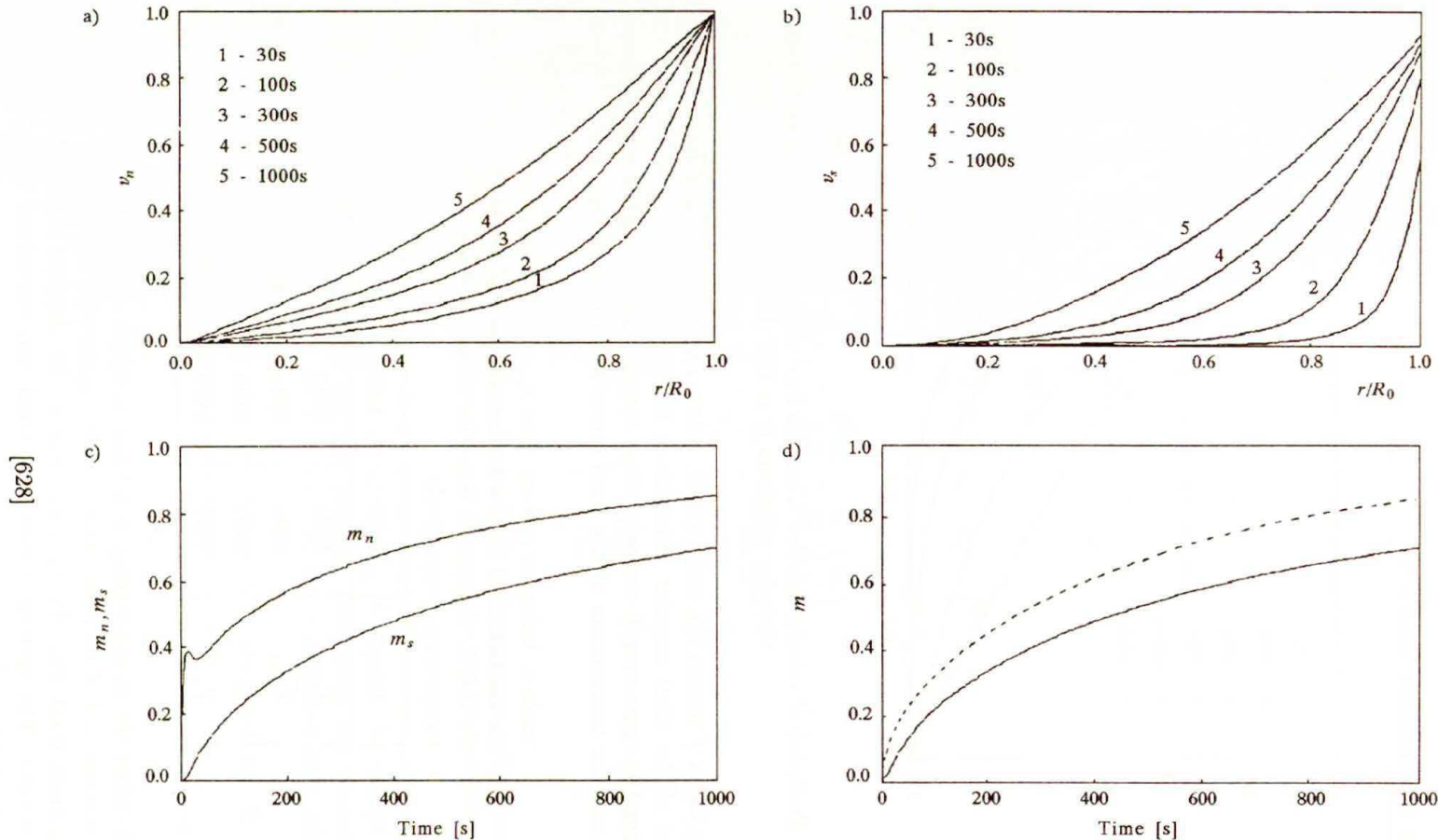


FIG. 7. Temp. = 1.26° K. Evolution of normal (a) and superfluid (b) component velocity profiles. c) Time evolution of scaled angular momentum, upper curve – normal component, lower curve – superfluid component. d) Time evolution of total angular momentum, dotted curve – classical fluid with the same overall viscosity.

[629]

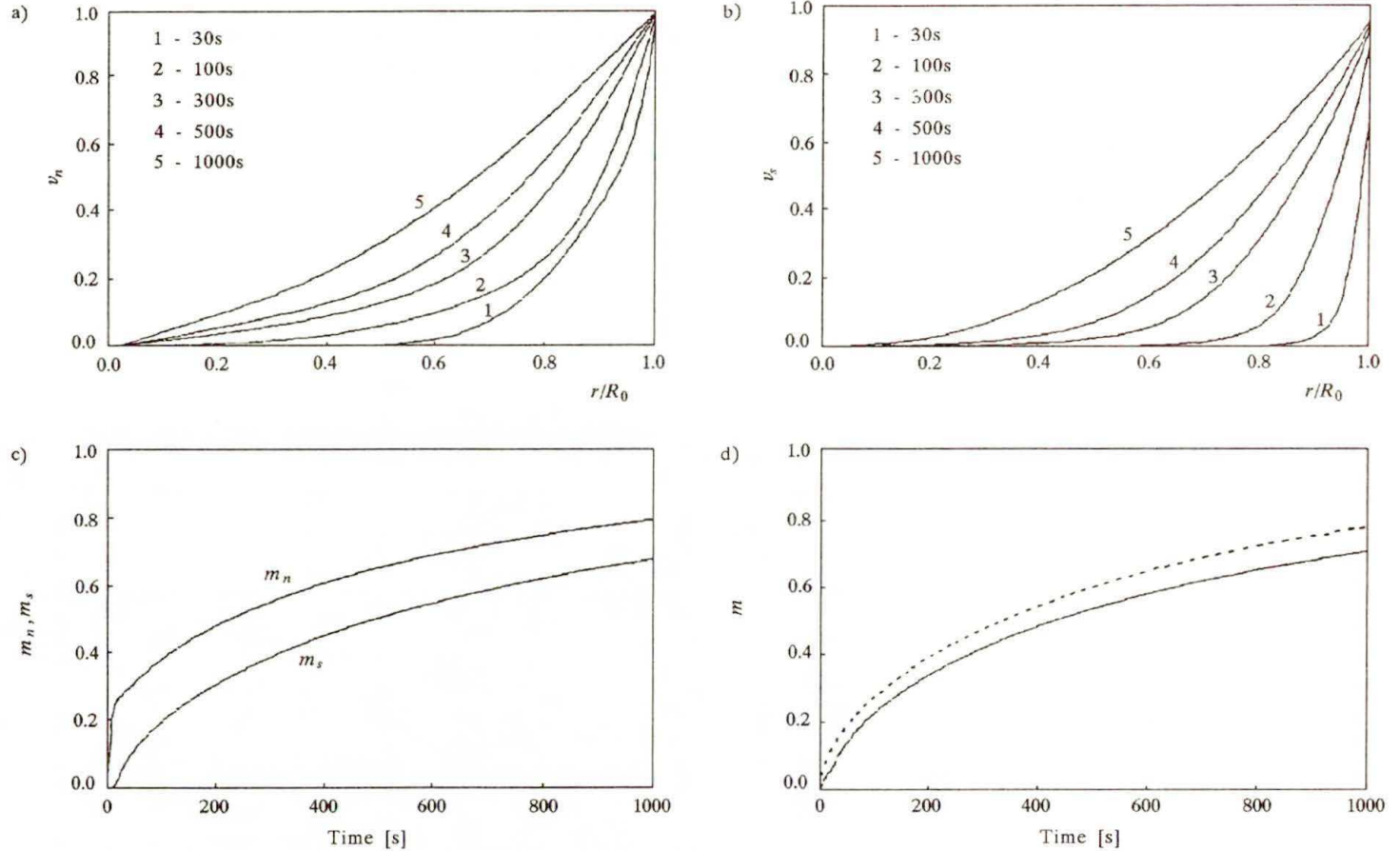


FIG. 8. Temp. = 1.62°K . Evolution of normal (a) and superfluid (b) component velocity profiles. c) Time evolution of scaled angular momentum, upper curve – normal component, lower curve – superfluid component. d) Time evolution of total angular momentum, dotted curve – classical fluid with the same overall viscosity.

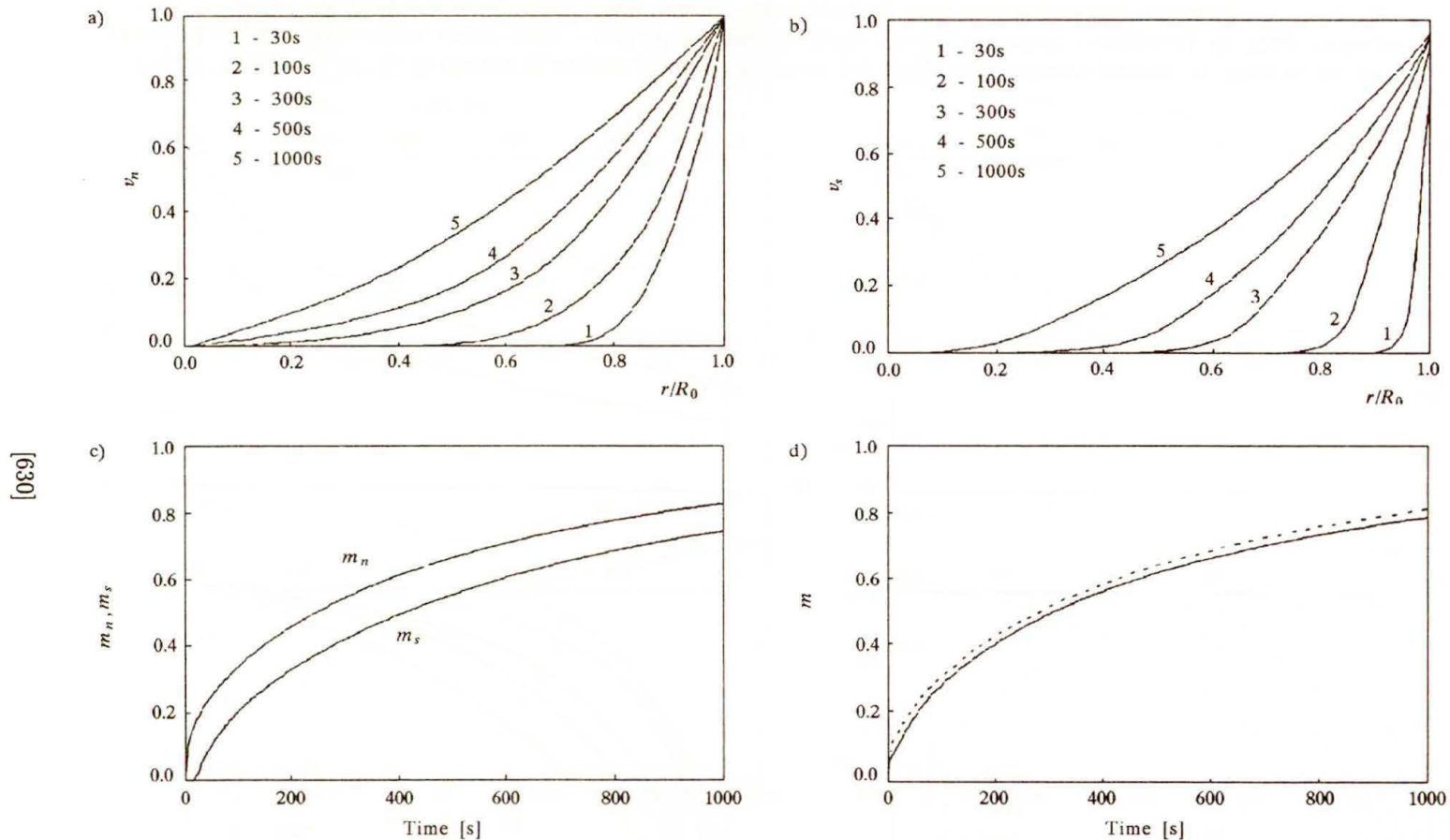


FIG. 9. Temp. = 2.01°K . Evolution of normal (a) and superfluid (b) component velocity profiles. c) Time evolution of scaled angular momentum, upper curve – normal component, lower curve – superfluid component. d) Time evolution of total angular momentum, dotted curve – classical fluid with the same overall viscosity.

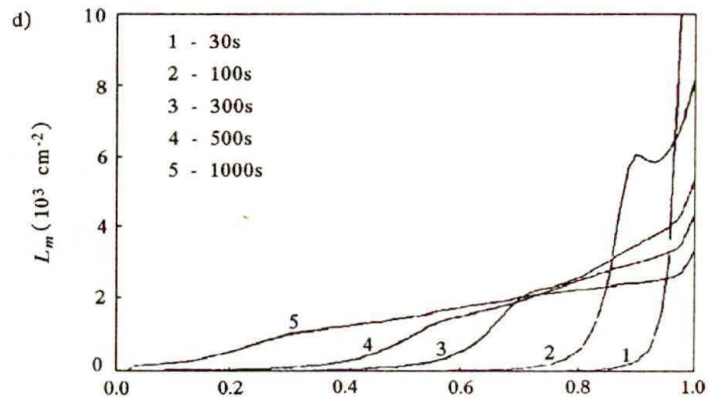
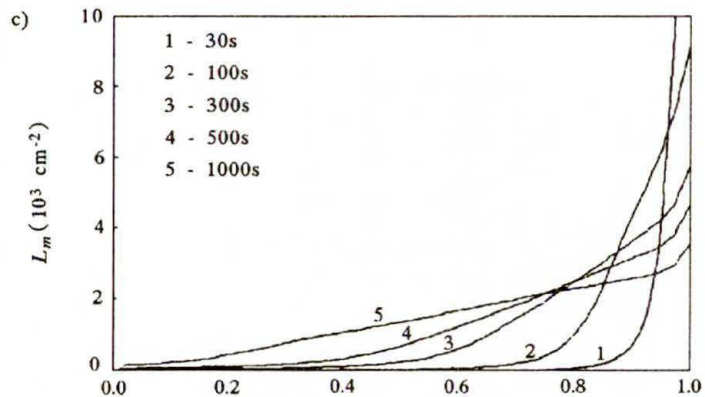
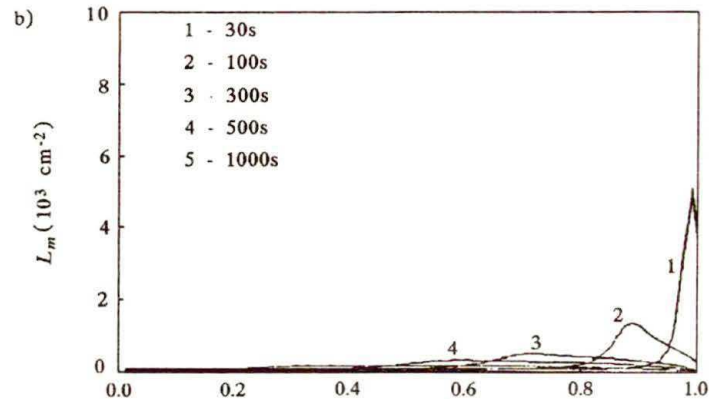
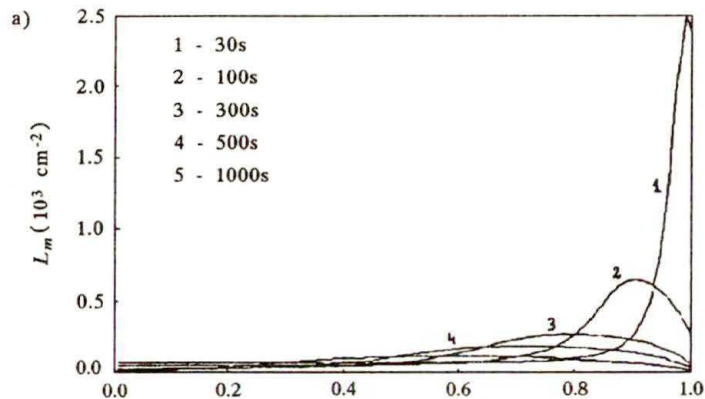


FIG. 10. Evolution of turbulent line-length density L_m , a) Temp. = 1.62 b) Temp. = 2.01 and parallel vortex line-length density L_{\parallel} , c) Temp. = 1.62, d) Temp. = 2.01.

6. Conclusions

The presented mechanism of the spin-up process, based on the Vinen model, can be summed up as follows. When the cylinder starts moving, it drags the normal viscous component of helium II. Then according to Vinen equation (1.3), relative velocity of the two components gives rise to quantum turbulence. The mutual friction force caused by the turbulence couples the components, and the superfluid starts spinning. After a sufficiently long time both components will rotate as a rigid body (with the same velocities) and the turbulent vortex line-length density will decrease (according to Vinen equation) to zero. This cannot be of course satisfied, because the spinning superfluid component has to contain vortices. Their minimum length density $L_{||}$ (in the case when they are parallel) is

$$(6.1) \quad L_{||} = \frac{\omega}{\kappa}.$$

In the considered case the final value of $L_{||}$ is $2000/\text{cm}^2$. Moreover one can see in Fig. 10 that the turbulent line-length density is much smaller than the “parallel vortex” line-length density calculated from superfluid velocity profiles. On the one hand, the large density of parallel vortices is due to the fact that mutual friction force makes the superfluid velocity profiles very steep. On the other hand, the Vinen equation (1.3) does not explain how such number of vortices may arise.

It can be clearly seen now that the Vinen model (in the present shape) cannot describe the turbulent flow which arises in the spinning cylinder. However, the first 3 examples show that the spin-up process is dominated by quickly arising turbulence. It points that the more accurate model should be rather based on the Vinen model than on the HVBH one (the analysis of spin-up in the HBVK model may be found in [10]).

The modified model should be related to the following facts:

1. The parallel vortices cannot decay unless the net superfluid vorticity change. Hence the second term in Vinen Equation has to be modified. The production of turbulent vortices due to the counterflow (first term in Vinen Equation) may be also influenced by an array of parallel vortices.

2. When the superfluid is dragged by normal component and starts spinning, the “turbulent vortices” have to change into locally parallel vortices. This means the negative source of turbulent vortices.

3. The Magnus force acting on the vortex tangle with a net vorticity makes that the vortex tangle moves across the counterflow; in the considered case inward the cylinder.

Pinning is the other important phenomena which may significantly influence the spin-up process. Quantum vortices pinned to the vessel boundaries may transfer the angular momentum directly from the cylinder to the superfluid component

(see [11]). This may be especially important in low temperatures when the normal component is less abundant.

Coming back to the entrainment and spin-up problem, we recall that the entrainment time scale $T_{\text{ent}} \sim V_0^{-2}$, where V_0 is characteristic counterflow velocity. This means that in experiments with larger velocities, the dynamics of helium II should be closer to the dynamics of classical fluid with the same overall viscosity.

Acknowledgments

Author is grateful to Prof. Z. PERADZYŃSKI for helpful discussion.

References

1. L. LANDAU, *J. Phys.*, **5**, 71, 1941.
2. L. ONSAGER, *Nouovo Cimento*, **6**, 249, 1949.
3. R.P. FEYNMAN, [in:] *Progress in Low Temperature Physics*, Vol. I, p.17, C.J. GORTER [Ed.] North-Holland, Amsterdam 1955.
4. W.F. VINEN, *Proc. R. Soc. London*, **A 240**, 114, (**240**, 128), (**242**, 493) 1957.
5. I.L. BEKAREVICH and I.M. KHALATNIKOV, *Sov. Phys. JETP*, **13**, 643, 1961.
6. K.W. SCHWARZ, *Phys. Rev.*, **B 38**, 2398, 1988.
7. K.W. SCHWARZ and J.R. ROZEN, *Phys. Rev.*, **B 44**, 7563, 1991.
8. J.A. GEURST and H. VAN BEELEN, *Physica*, **B 205**, 209, 1995.
9. S.K. NEMIROWSKII and D.W. SCHMIDT, [in:] *Reflections on Some Problems Concerning the Role of Superfluid Turbulence*, Max-Planck-Institut für Strömungsforschung, Bericht 8/1990.
10. Z. PERADZYŃSKI, S. FILIPKOWSKI and W. FISZDON, *Eur. J. Mech., B/Fluids*, **9**, 3, 259, 1990.
11. P.W. ADAMS, M. CIEPLAK and W.I. GLABERSON, *Phys. Rev.*, **B 32**, 1, 171, 1985.

POLISH ACADEMY OF SCIENCES

INSTITUTE OF FUNDAMENTAL TECHNOLOGICAL RESEARCH

e-mail: tlipnia@ippt.gov.pl

Received November 8, 1996.
